Kinetic study of oxidative dehydrogenation of ethane over MoVTeNb mixed oxide catalyst

ARTICLE · OCTOBER 2013

I&EC research
Industrial & Engineering Chemistry Research

Article

pubs.acs.org/IECR

Kinetic Study of Oxidative Dehydrogenation of Ethane over MoVTeNb Mixed-Oxide Catalyst

Jaime S. Valente,*[,†] R. Quintana-Solórzano,*[,†] H. Armendáriz-Herrera,[†] G. Barragán-Rodríguez,[†] and J. M. López-Nieto[‡]

[†]Instituto Mexicano del Petróleo, Eje Central Lázaro Cárdenas N°152, México, DF, CP 07730, Mexico

[‡]Instituto de Tecnología Química, UPV-CSIC, Campus de la Universidad Politécnica de Valencia, Av. de los Naranjos S/N, 46022 Valencia, Spain

Supporting Information

ABSTRACT: A MoVTeNb multimetallic mixed oxide was studied for the oxidative dehydrogenation of ethane, a promising alternative for catalytic ethylene production. Lab-scale steady-state experimental reaction data were obtained according to a 3^k experimental design to investigate the simultaneous effect of temperature (400−480 °C) and space−time [23−70 g_{cat} h (mol of ethane)$^{-1}$]. A fixed-bed reactor at atmospheric pressure was employed, feeding a mixture of ethane, oxygen, and nitrogen. Ethane conversion varied from 17 to 85%, whereas selectivity for ethylene and CO_x varied from 94 to 76% and from 4.0 to 24%, respectively. These types of analyses are useful for determining the optimum reaction conditions to enhance the catalytic performance of the mixed oxides presented herein.

1. INTRODUCTION

Ethylene is the most important olefin in the petrochemical context, as it is the major raw material for the production of polymers. At present, commercial ethylene is obtained worldwide mainly from the steam cracking of hydrocarbon cuts (e.g., ethane, naphtha, gas oils, etc.), with a small contribution from the fluid catalytic cracking of gas oils (FCC process). The ethylene market follows an increase related to world population growth; hence, the demand for ethylene is expected to increase continuously in the coming years.[1]

Currently, the main industrial process for ethylene production is steam cracking. This is a thermal conversion process carried out at high temperatures (800−900 °C).[2] Hence, the associated energy demand is considerably large. Also, special metallurgy is required for the internal components of the furnace, and the high operating temperature increases the occurrence of side reactions. Thus, the global selectivity for ethylene is reduced, and a large diversity of byproducts is obtained (e.g., acetylene, methane, propane, butane, etc.). The downstream separation scheme is therefore relatively complex.[3,4]

Catalytic dehydrogenation of ethane is also very demanding in terms of energy, due to the thermodynamic limitations associated with the endothermic nature of the reaction ($\Delta H^{o}_{R,298K}$ = 135.9 kJ mol^{-1}; $\Delta G^{o}_{R,298K}$ = 100.3 kJ mol^{-1}). The reaction must be performed above 700 °C to be commercially attractive.[5] Direct dehydrogenation of ethane has been improved with the incorporation of active and selective catalysts; however, these catalysts are susceptible to deactivation by coke (a high molecular mass side product inevitably formed in the course of the reaction).[6] Concerning the FCC process, it is aimed at producing gasoline and diesel oil as well as C_3−C_4 olefins; hence, ethylene is produced in relatively low amounts.

In view of the various disadvantages described above, combined with a worldwide interest in increasing ethylene production and the gradual increase in demand for petroleum-based products, it is urgent to develop new alternatives for ethylene production.[3−5] For several years now, the investigation of the oxidative dehydrogenation (ODH) of ethane has been a subject of great interest. The ODH of ethane is performed over a solid catalyst wherein ethane reacts with an oxidant species, typically oxygen.[5] Several advantages are noticed when comparing the ODH of ethane to the existing commercial processes.[7] In the ODH of ethane process, (i) no thermodynamic limitations exist ($\Delta G^{o}_{R,298K}$ = −128 kJ mol^{-1}), (ii) the reaction is exothermic ($\Delta H^{o}_{R,298K}$ = −106 kJ mol^{-1}), eliminating the need for an external heat supply, (iii) a limited number of reaction products are observed (mainly CO_x, aside from ethylene), and (iv) no catalyst deactivation by coke is expected, owing to the oxygen present in the reaction medium. Commercial production of ethylene via the ODH of ethane remains a challenge.[2,5] The key lies in developing a catalyst with adequate properties: the catalyst should be able to transform ethane at low temperatures to produce ethylene while minimizing the formation of CO_x. An attractive scenario reported for the ODH of ethane presents ethylene selectivity larger than 90% and ethane conversion greater than 60% at temperatures lower than 500 °C.[2,3] High selectivity for ethylene is one of the most important features of a suitable catalyst, not only for economic feasibility, but also because the combustion reactions responsible for the formation of CO and CO_2 are ca. 8 and 13 times more exothermic, respectively, than they are for the production of ethylene from ethane. This represents an important issue for operational reactor control, due to the hot points

Special Issue: Recent Advances in Natural Gas Conversion

Received: July 30, 2013
Revised: September 9, 2013
Accepted: September 10, 2013

   dx.doi.org/10.1021/ie402447h | *Ind. Eng. Chem. Res.* XXXX, XXX, XXX−XXX

generated by the aforementioned combustion reactions. Aimed at fulfilling both activity and selectivity requirements, a large variety of catalytic systems have been proposed.[4−6,8,9] Thus far, one of the most efficient and promising catalysts for partial oxidation reactions, particularly for the ODH of ethane, is a multimetallic mixed oxide that contains Mo, Te, V, and Nb, which has been described and studied by several research groups.[10−17]

MoTeVNb-based materials consist of a mixture of crystalline phases, mainly two, denoted as M1 and M2[10−21] in the scientific literature. The M1 phase was shown to be mainly responsible for the activity, as it holds the active and selective surface sites needed for the partial oxidation of ethane.[11−17,21−23] The activation of this catalytic formulation occurs at around 350 °C, exhibiting acceptable values of ethane conversion with a remarkably high selectivity for ethylene. Even though some information concerning the effects of temperature and other important operating conditions on the performance of these catalysts for the ODH of ethane has been reported in literature,[5,11−14,21−23] to the best of our knowledge no reports have been published for the MoTeVNb mixed-oxide catalytic system in particular, correlating the kinetic aspects of the ODH of ethane with temperature, space−time, and ethane and oxygen inlet partial pressures.

Where kinetic models are concerned, few models have been proposed to describe the ODH of ethane over different types of catalytic systems by applying the power law, Langmuir−Hinshelwood, Eley−Rideal, and Mars−Van Krevelen formalisms.[24−32] Each kinetic model is specific for a given catalytic formulation; hence, the available published information related to the kinetic parameters (i.e., activation energies, pre-exponential factors) as well as adsorption parameters is diverse.

The aim of this work is to elucidate the effects of temperature, space−time, and ethane and oxygen inlet partial pressures on the steady-state catalytic performance of the MoVTeNb multimetallic mixed oxide for the ODH of ethane to ethylene. The effects of temperature and space−time, two of the most important variables in the operation of catalytic reactors, were assessed by applying a 3^k experimental design. A statistical analysis of the experimental design was carried out to determine the significance of the main factors, their effects, and their interaction on a set of selected catalytic responses. Next, 3D surface plots were used to explore convenient regions of operation for some representative catalytic responses, such as ethane conversion, ethylene selectivity, CO_x selectivity, and the space time yield (STY) of ethylene. Therefore, a power law-based kinetic model was developed by varying the reaction temperature from 400 to 480 °C, the space−time ($w_{cat}F_{ethane,o}^{-1}$) from 10 to 140 g_{cat} h (mol of fed ethane)$^{-1}$, and the ethane and oxygen inlet partial pressures from 5.1 to 22.3 kPa. Although power law-based kinetics disregard mechanistic aspects, they are extensively used for reactor scale-up and design.

2. EXPERIMENTAL PROCEDURES

2.1. Catalysts Preparation. A MoVTeNb multimetallic mixed oxide with the nominal atomic ratios of Mo:V:Te:Nb = 1:0.24:0.24:0.18 was prepared. Briefly, the synthesis of the catalyst involved the following steps: (i) an aqueous solution containing tetrahydrated ammonium heptamolybdate (Merck, 99%), telluric acid (Aldrich, 98%), and ammonium metavanadate (Sigma-Aldrich, 99.5%) was prepared under continuous stirring at 80 °C; separately, (ii) an aqueous solution of niobium oxalate (ABCR Laboratories, 99%) and oxalic acid (Aldrich, 98%) was prepared, also at 80 °C. Solution (ii) was added to the solution of step (i) while a vigorous continuous stirring was maintained. The resulting mixture transformed into a slurry, which was cooled to room temperature. Then, the pH of the slurry was adjusted to 2.5 by adding 1 M nitric acid solution. The acidified slurry was subsequently placed in a rotavapor system at 50 °C and 27 kPa to gradually evaporate the water. The resulting powder was dried overnight at 100 °C and then thermally treated at 600 °C for 2 h under nitrogen flow.

2.2. Catalyst Characterization. The catalyst was characterized by X-ray power diffraction in a Siemens D-500 diffractometer provided with a $\theta-\theta$ configuration and a graphite secondary-beam monochrome. Diffraction was measured from 4 to 80° with a 2θ step of 0.02° for 8 s per point, using Cu $K\alpha_{1,2}$ radiation with a wavelength of 1.5418 Å as well as a power of 40 kV and 40 Ma. The M1 and M2 phases were refined by using the Rietveld method with help from the MAUD Bruker program. The full pattern was fitted according to the M1 and M2 orthorhombic crystal structures (space group *Pba*2 no. 32; ICSD 55097) to determine the percentage of crystalline phases present in the catalysts.

The chemical composition of the solids was determined in a Perkin-Elmer OPTIMA 3200 Dual Vision by inductively coupled plasma atomic emission spectrometry (ICP-AES).

The specific surface area of the calcined powdered catalyst was analyzed by N_2 physisorption at −196 °C on an AUTOSORB-I apparatus. Prior to the analysis, the sample was outgassed in a vacuum (10^{-5} Torr) at 300 °C for 5 h. The specific surface area was calculated by using the Brunauer−Emmett−Teller (BET) method.

2.3. Catalytic Testing. *2.3.1. Reactor and Chromatographic Setup.* The catalytic experiments were performed in a semiautomatized lab-scale setup, equipped with a fixed-bed quartz tubular reactor having an internal diameter of 10 mm and length of 200 mm, operated isothermally at atmospheric pressure and integral regime. The reactor was provided with two thermocouples, one indicating the reactor wall temperature and the other measuring the catalyst bed temperature. All runs were performed by feeding the reactor with a mixture consisting of ethane (C_2) and oxygen (O_2), as well as nitrogen (N_2) as diluent. The N_2 was also employed as an internal standard. The purities of ethane, oxygen, and nitrogen utilized in the experiments were 99.7 vol %, 99.996 vol %, and 99.999 vol %, respectively. The flow rate of the gases was quantified by using independent thermal mass flow controllers (MFC) Brooks 5850I.

The reactor effluent was analyzed online periodically by gas chromatography (GC). Said analysis was conducted in a HP-7890 series II GC equipped with a flame ionization detector (FID) and a thermal conductivity detector (TCD), with an array of three columns: a 30 m × 530 μm × 50 μm HP Plot Q capillary, a 30 m × 530 μm × 40 μm molecular sieve, and a 30 m × 0.25 mm × 5 μm HP Plot alumina. Although hydrocarbons are observable in both the TCD and the FID, they were quantified in the FID owing to the higher sensitivity of this detector to these compounds. The other reaction products, namely, CO_2 and CO, as well as oxygen and nitrogen, were identified in the TCD.

2.3.2. Operating Conditions. For a typical experiment, 0.60 g of thermally treated catalyst with an average particle size of 150 μm was loaded into the reactor. Before reaction testing, the composition of the gaseous mixture was verified by GC, and it was preheated at 140 °C. The reactor was heated with a furnace and set to the intended temperature. A blank experiment, carried out at 480 °C, confirmed the absence of both ethane

dx.doi.org/10.1021/ie402447h | Ind. Eng. Chem. Res. XXXX, XXX, XXX−XXX

and oxygen conversions in the absence of catalyst. The reaction was followed for 6 h. In all experiments, the carbon balance reported values within the range of 100% ± 2.0%.

For a systematic investigation of the concomitant influence of temperature and space−time on the catalytic behavior of the MoVTeNb catalyst, a first set of experiments was performed in accordance with a factorial experimental design. Here, the inlet partial pressures of ethane, oxygen, and nitrogen were fixed at 7.0, 5.5, and 65.5 kPa, respectively. Since a nonlinear effect of temperature over some responses is expected, and considering that only two independent factors will be studied, a 3^k design was proposed, k being the number of independent factors and "3" denoting the number of levels of the factors explored. The specific levels of the factors, temperature and space−time in this case, are denoted as low (0), medium (1), and high (2) for the lowest, intermediate, and highest values of the factor, respectively. Specifically, the temperature was varied from 400 to 480 °C, and space−time was varied between 23 and 70 g_{cat} h (mol of fed ethane)$^{-1}$. The number of combinations between the factors and the corresponding levels is 9 (3^2), denoting the number of independent experiments to be performed for a genuine replicate (n). Aimed at calculating the error of the experimental design, two genuine replicates, $n = 2$, were accounted for. Independent variables, other than temperature and space−time, were kept at the values outlined in section 2.3.2. The maximum operation temperature was set to 480 °C. Even though several catalytic responses (e.g., conversion, selectivity, yield, etc.) could be considered in the experimental design, only four responses were taken into account (vide infra).

In a second set of experiments carried out at 440 °C, the inlet partial pressure of ethane ($P^o_{C_2}$) was varied at constant inlet partial pressure of oxygen ($P^o_{O_2}$), and vice versa. To obtain values of the overall rates, space−time was also changed in this set. The inlet partial pressures of ethane and oxygen were ranged from 5.1 to 22.3 kPa, whereas space−time was varied from 10 to 140 g_{cat} h (mol of fed ethane)$^{-1}$. With these operating conditions, the ratio of ethane to oxygen in the feed varies from 0.5 to 2.0.

An assessment of the transport limitations for the main reaction was performed in accordance with the different criteria reported in literature.[33,34] Concentration and temperature gradients were found to be below the suggested limits,[34] while the criteria for plug-flow mode and isobaric operation at the reactor bed scale were also fulfilled.

2.3.3. Calculations of the Value of Responses Considered in the Experimental Design. The factors selected in the experimental design were ethane conversion, ethylene selectivity, and the STY of ethylene. Ethane conversion and ethylene selectivity were defined on a carbon basis. Ethane conversion was calculated by eq 1:

$$X_{C,ethane}\ \% = \frac{G^o_{C,ethane} - G_{C,ethane}}{G^o_{C,ethane}} 100 \tag{1}$$

where $G^o_{C,ethane}$ and $G_{C,ethane}$ denote the mass flow of ethane at the inlet and outlet of the reactor, respectively.

Selectivity for ethylene and for the oxidation products CO and CO_2 were computed considering the carbon mass in component i formed per mass of carbon in ethane converted according to eq 2:

$$S_{C,i}\ \% = \frac{G_{C,i}}{G^o_{C,ethane} - G_{C,ethane}} 100 \tag{2}$$

The ethane flow at the reactor entrance, quantified by the MFC, was measured at standard conditions, namely, 1 atm (101.32 kPa) and 20 °C. The flow at the reactor outlet was quantified via the internal standard method according to eq 3:

$$F_i = \frac{F^o_{N_2} M_{N_2}}{A_{N_2} Cf_{N_2}} \frac{A_i Cf_i}{M_i} \tag{3}$$

where F_i is the outlet molar flow rate of compound i, calculated from the molecular mass (M_i), the GC-integrated area (A_i), and the GC-calibration factor (Cf_i) of product i; the corresponding values of nitrogen were used as an internal standard ($F^o_{N_2}$ is the molar flow rate).

The carbon flow of compound i, at the reactor outlet, is calculated by considering the number of carbons in the molecule as well as carbon's atomic mass, by eq 4.

$$G_{C,i} = 12 F_i C_{atoms,i} \tag{4}$$

The third factor, accounting for the STY of ethylene, is defined as the grams of ethylene produced per hour and per kilogram of catalyst (w_{cat}). It is calculated by means of eq 5.

$$STY = \frac{F_{ethylene} M_{ethylene}}{w_{cat}} \tag{5}$$

2.4. Kinetic Modeling. *2.4.1. Reaction Network and Rate Expressions.* The reaction network employed for the kinetic modeling of the ODH of ethane is presented in Scheme 1. In

Scheme 1. Reaction Network Employed for the Kinetic Modeling of Ethane ODH

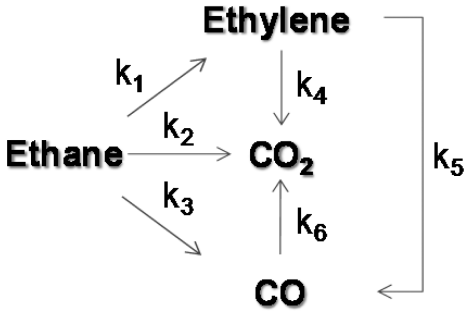

accordance with this scheme, ethane reacts with oxygen to produce ethylene and CO_2 as well as CO. Produced ethylene is susceptible to subsequent reactions, converting it into CO_2 and/or CO. The transformation of CO to CO_2 was found to be a nonsignificant step on the basis of statistical information obtained in the parameter estimation procedure, namely, t-Student based confidence intervals; hence, it was not considered in the reaction network equations. The reaction rates are described by power law rate equations; hence, a rate coefficient is included, as are the partial pressures of the reagents (ethane, ethylene, and oxygen) and the reaction orders for each reagent. For the species involved in the network, their overall rates are expressed by eqs 6−9.

$$R_{ethane} = -(k_1 P^{\alpha_1}_{ethane} P^{\beta_1}_{oxygen} + k_2 P^{\alpha_2}_{ethane} P^{\beta_2}_{oxygen} + k_3 P^{\alpha_3}_{ethane} P^{\beta_3}_{oxygen}) \tag{6}$$

$$R_{ethylene} = k_1 P^{\alpha_1}_{ethane} P^{\beta_1}_{oxygen} - k_4 P^{\alpha_4}_{ethylene} P^{\beta_4}_{oxygen} - k_5 P^{\alpha_5}_{ethylene} P^{\beta_5}_{oxygen} \tag{7}$$

dx.doi.org/10.1021/ie402447h | Ind. Eng. Chem. Res. XXXX, XXX, XXX−XXX

$$R_{CO_2} = 2.0(k_2 P_{ethane}^{\alpha_2} P_{oxygen}^{\beta_2} + k_4 P_{ethylene}^{\alpha_4} P_{oxygen}^{\beta_4}) \quad (8)$$

$$R_{CO} = 2.0(k_3 P_{ethane}^{\alpha_3} P_{oxygen}^{\beta_3} + k_4 P_{ethylene}^{\alpha_5} P_{oxygen}^{\beta_5}) \quad (9)$$

where α_1, α_2, ..., α_5 are the reaction orders related to the partial pressure of hydrocarbon (ethane or ethylene), while β_1, ..., β_5 denote the reaction orders associated with the partial pressure of oxygen, which must be determined experimentally.

For oxygen and water, which were not explicitly included in the network of Scheme 1, the corresponding overall rates are given by eqs 10 and 11.

$$R_{O_2} = -0.5k_1 P_{ethane}^{\alpha_1} P_{oxygen}^{\beta_1} - 3.5k_2 P_{ethane}^{\alpha_2} P_{oxygen}^{\beta_2} - 2.5k_3 P_{ethane}^{\alpha_3} P_{oxygen}^{\beta_3} - 3.0k_4 P_{ethylene}^{\alpha_4} P_{oxygen}^{\beta_4} - 2.0k_5 P_{ethylene}^{\alpha_5} P_{oxygen}^{\beta_5} \quad (10)$$

$$R_{H_2O} = k_1 P_{ethane}^{\alpha_1} P_{oxygen}^{\beta_1} + 3.0(k_2 P_{ethane}^{\alpha_2} P_{oxygen}^{\beta_2} + k_3 P_{ethane}^{\alpha_3} P_{oxygen}^{\beta_3}) + 2.0(k_4 P_{ethylene}^{\alpha_4} P_{oxygen}^{\beta_4} + k_5 P_{ethylene}^{\alpha_5} P_{oxygen}^{\beta_5}) \quad (11)$$

The constants k_i used in eqs 6−11 are the rate coefficients (i = 1, 2, ..., 5) denoting the reaction according to the assigned number in Scheme 1. They are temperature-dependent, calculated in accordance with the Arrhenius expression of eq 12.

$$k_i = A_i \exp(-E_i/RT) \quad (12)$$

where E_i is the activation energy and A_i is the pre-exponential factor of i. The determination of E_i and A_i, with corresponding statistics, is accomplished by using experimental data at different temperatures.

To reduce the initial correlation of pre-exponential factors with activation energies, the pre-exponential factors were used in the reparameterized form. Consequently, the rate coefficient of reaction i was computed according to the reparameterized Arrhenius expression by eq 13.

$$k_i = A_{rep,i} \exp\left(\frac{E_i}{R}\left[\frac{1}{T_m} - \frac{1}{T}\right]\right) \quad (13)$$

The reparameterized pre-exponential factor designated $A_{rep,i}$ is calculated by using eq 14.

$$A_{rep,i} = A_i \exp\left(-\frac{E_i}{RT_m}\right) \quad (14)$$

where T_m is the mean temperature.

2.4.2. Reactor Model Equations and Parameters Estimation. Parameter estimation was performed by minimizing the weighted sum of squares of the residuals (RSS) between the kinetic model predicted yields, referred to as $\hat{Y}_{i,j}$, and the experimental molar yields, designated Y_{ij}, for the species of the reaction network of Scheme 1, according to eq 15.

$$RSS(\beta) = \sum_{i=1}^{n_{obs}} \sum_{j=1}^{n_{resp}} w_j (Y_{i,j} - \hat{Y}_{i,j})^2 \xrightarrow{\beta_1, \beta_2, \ldots \beta_{np}} \min \quad (15)$$

where β is the vector of kinetic parameters estimated via regression, n_{obs} is the number of independent experiments, n_{resp} is the number of responses, n_p is the number of parameters, and w_j is a weight factor that can be optionally used for tuning the relative importance of the various responses. For an experiment i, the experimental molar yield of a species j was calculated by the eq 16.

$$Y_{i,j}\,\% = \frac{F_{i,j}}{F_{i,ethane}^{o}} 100 \quad (16)$$

The predicted yields considered in the objective function were obtained according to eq 17, via numerical integration of the corresponding reactor model equations, given in a set of ordinary differential equations (ODEs).

$$R_{i,j} = \frac{d\hat{Y}_{i,j}}{d(w_{cat} F_{ethane,o}^{-1})_i} \quad (17)$$

with $Y_{i,j}(0) = 0.0$ as a boundary condition for experiment i and species j. For the i^{th} experiment, the overall rate formation of species j represented by $R_{i,j}$ is given by eqs 6−11.

Equation 17 describes a continuous pseudohomogeneous, isothermal, isobaric 1D plug flow reactor, operated in the integral regime, in the absence of concentration and thermal gradients. Numerical integration of the ODEs given by eq 17 was carried out by using the routine of the Livermore solver for ordinary differential equations that automatically selects between nonstiff and stiff methods (LSODA).[35]

The package of software for the orthogonal distance regression problem (ODRPACK 2.01 solver)[36] was used to obtain the parameters that minimize the objective function (vide eq 14) by nonlinear ordinary least-squares for explicit models, with an implementation of the Levenberg−Marquardt method. In a first stage, rate coefficients were estimated at each temperature in order to obtain initial values for the activation energies and pre-exponential factors using Arrhenius-type plots. In a second stage, the temperature dependence of the parameters was calculated by using the experimental data at all temperatures and estimating directly the values of activation energies and reparameterized pre-exponential factors. To assess the parameter estimation results, the F-test for the global significance of the regression and the individual confidence intervals based on the t-test for the estimates were computed.

2.4.3. Apparent Reaction Orders. In the case of a multireaction system, contrary to what occurs in a single reaction case, the reaction orders associated with each reaction are not directly accessible from experimental data. Instead, kinetic orders for the various reactants can be determined from the corresponding overall reactions considering they can also be expressed in terms of a power law kinetic formalism, as expressed by eq 18 for a species j:

$$R_j = \sum_{i=1}^{n_r} k_i P_{ethane}^{\alpha_i} P_{O_2}^{\beta_i} = k_j P_{ethane}^{m_j} P_{O_2}^{n_j} \quad (18)$$

The overall rate of species j takes into consideration the contribution of all the reactions of species i (i = 1, 2, ..., n_r). The kinetic orders for the species are now n_j and m_j, the former being associated with the partial pressure of ethane and the latter with the partial pressure of oxygen. Thus, the kinetic orders related to ethane are calculated from experiments varying P_{ethane}^{o} at a given value of $P_{O_2}^{o}$; the reaction orders of oxygen are computed via experiments modifying $P_{O_2}^{o}$ maintaining constant the value of P_{ethane}^{o}. Taking the natural logarithm of both sides of eq 18 and varying, for instance, only the inlet partial pressure of oxygen results in eq 19.

$$\ln(R_j) = \text{constant} + n_j \ln(P_{O_2}) \quad (19)$$

dx.doi.org/10.1021/ie402447h | Ind. Eng. Chem. Res. XXXX, XXX, XXX−XXX

Experimental kinetic orders related to ethane and oxygen for a given product were then determined by applying the initial rates method.[36,37] Equation 17 is a continuity equation, a valid reaction model for a plug flow in the integral regime and in the absence of temperature and concentration gradients. Rate values are obtained from the first derivative of a space−time function expressed by the general form $Y = f(w_{cat}F_{ethane,o}^{-1})$. Initial rates are then obtained by evaluating the first derivative of Y at space−time equal to zero. Subsequently, fitting the $\ln(R_j^o)$ and the $\ln(P_{O_2}^o)$ data to a straight line gives a slope that corresponds to the n_j reaction order. A similar treatment is applied to the $\ln(R_j^o)$ and the $\ln(P_{ethane}^o)$ data to obtain the value of the m_j kinetic order, associated with the partial pressure of ethane.

3. RESULTS AND DISCUSSION

3.1. Characterization of the MoVTeNb Mixed-Oxide Catalyst. The main physicochemical properties of the thermally activated MoVTeNb mixed-oxide catalyst used for the kinetic study are reported in the Supporting Information. The specific surface area and the chemical composition of this material are comparable to those reported elsewhere for this type of solid.[14,38] Regarding the crystalline phase composition calculated by the Rietveld refinement, performed on the X-ray diffraction pattern shown in Figure 1, the predominant M1 phase is observed (92 wt %), to which the activity of this type of material is attributed.[11−17,21−23] Indeed, this material presents an outstanding catalytic performance, as shall be demonstrated in the following sections.

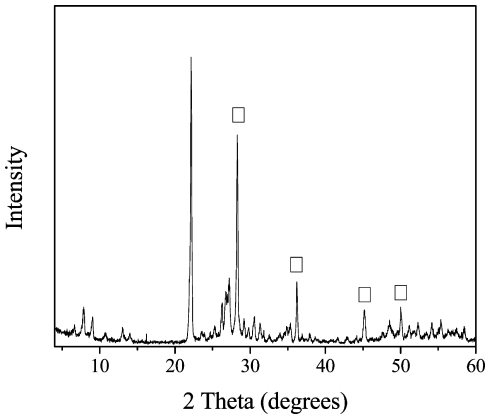

Figure 1. X-ray diffraction pattern of the thermally activated MoVTeNb mixed-oxide catalyst. In addition to the M1 phase the M2 phase (□) is also detected.

3.2. Catalytic Testing. During the catalytic experiments, a limited number of reaction products (ethylene, CO, and CO_2) were detected. Figure 2 shows the time-on-stream evolution of ethane and oxygen conversion as well as ethylene selectivity for an experiment performed at 440 °C and 35 g_{cat} h (mol of fed ethane)$^{-1}$. A remarkable catalytic stability is observed, as no significant changes in conversion and selectivity were detected during the six-hour reaction test. In this experiment, the catalyst exhibited a steady-state conversion of ethane as high as 48%, while the steady-state conversion of oxygen reached a value of around 36%. In addition, high ethylene selectivity, ca. 93%, was attained.

Qualitatively, the effluent composition was in the following order: ethylene ≫ CO > CO_2. The relative amounts of these compounds varied as a function of both temperature and space−time; ethylene was the main product while the formation of CO was always higher than that of CO_2. Results from the experiments performed at 400−480 °C, 23−70 g_{cat} h (mol of ethane)$^{-1}$, and an inlet molar ratio of $C_2/O_2/N_2$ = 9/7/84 showed that ethane conversion ranged from 17 to 85% and that of oxygen ranged from 17 to 96%. Concerning products distribution, as shown in Figure 3, selectivity for ethylene, CO, and CO_2 varied from 94 to 76%, 2.5 to 17%, and 1.5 to 7.5%, respectively. Additionally, the STY of ethylene, a key parameter of interest for the petrochemical industry, changed from 122 to 640 $g_{ethylene}$ (kg_{cat} h)$^{-1}$. Figure 3 displays the evolution of selectivity for ethylene, CO_2, and CO as a function of ethane conversion. Observe that, as the reaction conditions increase in severity in terms of temperature and space−time, ethane conversion and CO_x selectivity grow, to the detriment of selectivity for ethylene.

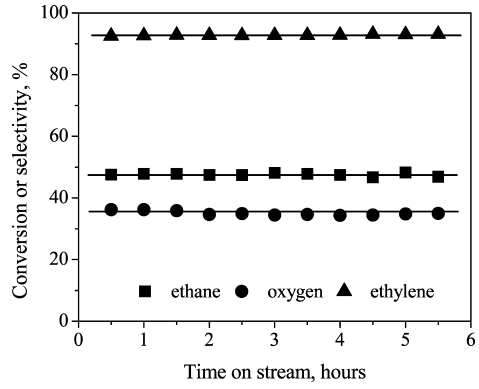

Figure 2. Ethane and oxygen conversions and ethylene selectivity. $T_{reaction}$ = 440 °C; space−time = 35 g_{cat} h (mol of ethane)$^{-1}$; inlet molar ratio $C_2/O_2/N_2$ = 9/7/84.

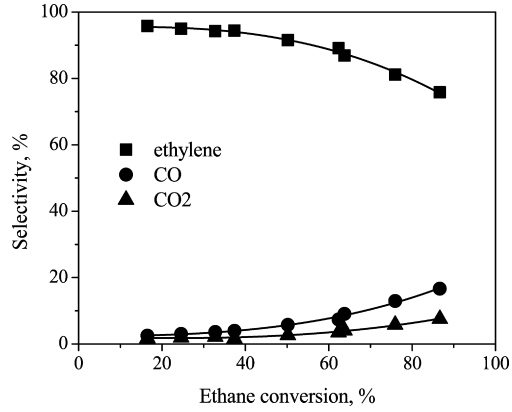

Figure 3. Variation of selectivity for ethylene, CO_2, and CO versus ethane conversion. $T_{reaction}$ = 400−480 °C; space−time = 23−70 g_{cat} h (mol of ethane)$^{-1}$; inlet molar ratio $C_2/O_2/N_2$ = 9/7/84.

3.3. Experimental Design Results. *3.3.1. Main Effects and Interactions.* As outlined previously, temperature (T) and space−time (w_{cat} $F_{ethane,o}^{-1}$), represented here as W, two key variables in the performance of catalytic reactors, were systematically studied by using reaction data generated in accordance with the 3^k factorial experimental design. Briefly, a select group of responses was considered, including ethane conversion, ethylene selectivity, and CO_x selectivity as well as the STY of ethylene. Since similar trends were observed for CO and CO_2, they were grouped into CO_x.

dx.doi.org/10.1021/ie402447h | Ind. Eng. Chem. Res. XXXX, XXX, XXX−XXX

A goal of an experimental design is to detect the extent of the influence of the most important factors on the considered responses. For a significant factor it is then necessary to identify the nature of its impact on the response and, further, to determine the interaction of this factor with others considered in the design.[39−41] Figure 4 contains a set of graphs exhibiting

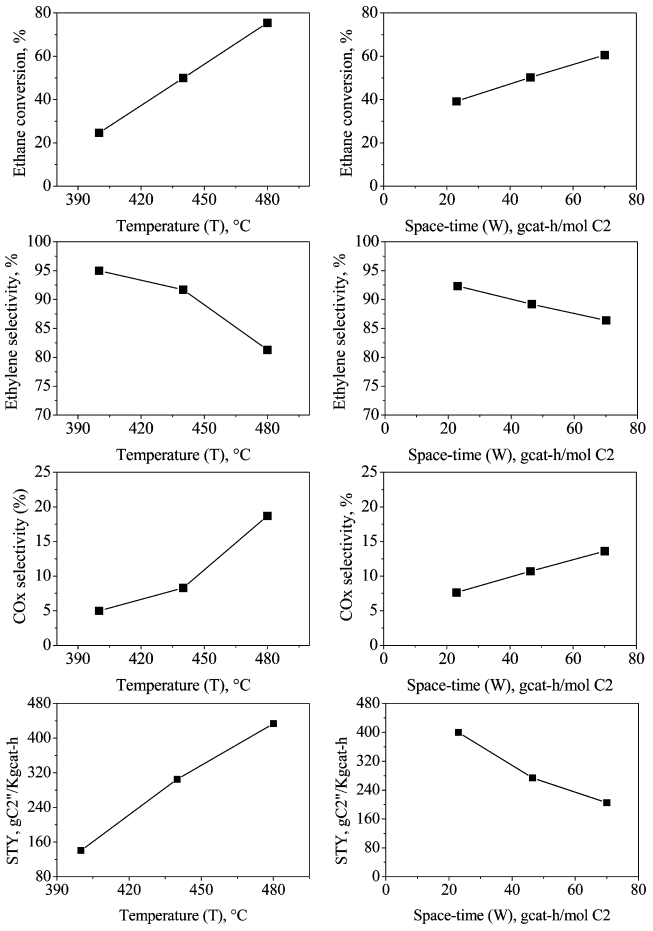

Figure 4. (from top panels to bottom) Main effects plot for ethane conversion, ethylene selectivity, CO_x selectivity, and the STY. From a 3^k factorial experimental design, temperature varied from 400 to 480 °C; space−time ranged between 23 and 70 g_{cat} h (mol of ethane)$^{-1}$; inlet molar ratio $C_2/O_2/N_2$ = 9/7/84.

the main effects for the four responses of interest. They are useful to visualize how the value of a response changes as a consequence of a continuous increase in the level of a given factor. Clearly, for ethane conversion and CO_x selectivity, increasing the level of both temperature and space−time positively effects the response. Selectivity for ethylene is, in contrast, negatively affected by increases in both temperature and space−time. The effects of increases in temperature and space−time on the STY have different signs, specifically, positive for the former and negative for the latter. On the basis of the slopes of these main-effect curves, we deduce that the various responses are not equally affected by the changes in the levels of temperature and space−time. Note that temperature has a strong effect on both ethane conversion and the STY, while space−time weakly affects ethylene selectivity.

When the average responses associated with one factor vary as a function of the level of the other factors, an interaction between factors occurs.[42,43] Figures 5 and 6 contain the

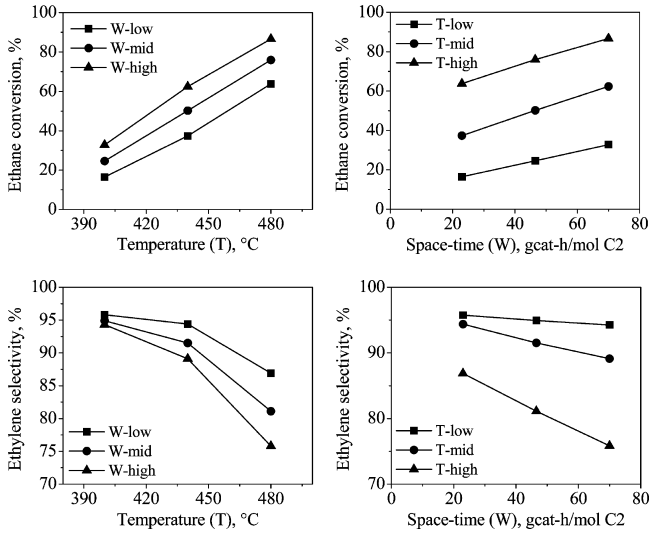

Figure 5. Interaction plots for (top panels) percent conversion of ethane and (bottom panels) ethylene selectivity. From a 3^k factorial experimental design, temperature varied (left panels) from 400 to 480 °C; space−time ranged (right panels) between 23 and 70 g_{cat} h (mol of ethane)$^{-1}$; inlet molar ratio $C_2/O_2/N_2$ = 9/7/84.

interaction plots for the studied responses. In the plots of conversion versus temperature and ethane conversion versus space−time (Figure 5), the three lines in each graph are parallel, corresponding to a case in which no interaction between the two factors occurs. The other interaction plots in Figure 5, for ethylene selectivity, and in Figure 6, for CO_x

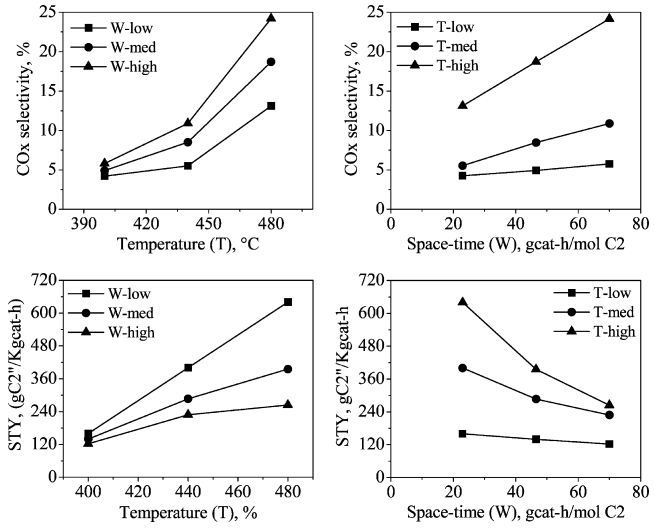

Figure 6. Interaction plots for (top panels) CO_x selectivity and (bottom panels) the STY. From a 3^k factorial experimental design, temperature varied (left panels) from 400 to 480 °C; space−time ranged (right panels) between 23 and 70 g_{cat} h (mol of ethane)$^{-1}$; inlet molar ratio $C_2/O_2/N_2$ = 9/7/84.

selectivity and the STY of ethylene, contrast with those for ethane conversion. The three lines in each of these graphs are not parallel, evidencing an interaction between temperature and space−time in each of these three responses.

On the basis of the interaction plots, the conclusive statements for the four responses analyzed are formulated as follows: (i) for ethane conversion, the effect of temperature and

dx.doi.org/10.1021/ie402447h | Ind. Eng. Chem. Res. XXXX, XXX, XXX−XXX

space−time is additive, whereas (ii) for ethylene selectivity, CO_x selectivity, and the STY of ethylene, the effect of space−time is nonadditive and depends on temperature. Specifically, selectivity for ethylene is negatively affected by space−time, and the value of this response decreases drastically as temperature increases, vide Figure 5. In the temperature range studied, the STY of ethylene decreases with space−time; however, at the low reaction temperature (400 °C) the STY of ethylene decline is slight, from 160 to 122 $g_{ethylene}$ $(kg_{cat}\ h)^{-1}$,when space−time rises from 23 to 70 g_{cat} h (mol of ethane)$^{-1}$. By contrast, at the high reaction temperature (480 °C), such a decrease is very pronounced, going from 640 to 264 $g_{ethylene}$ $(kg_{cat}\ h)^{-1}$, vide Figure 6.

3.3.2. Analysis of Variance. A more detailed inspection of both the main effects and the interactions is needed to define the extent to which the effects and interactions are statistically significant for a given response; to this end, performing an analysis of variance (ANOVA) is recommended.[37,38] The results of the ANOVA for ethane conversion are shown in Table 1. The ANOVA results for ethylene selectivity, CO_x selectivity, and the STY of ethylene are presented in the Supporting Information. In these results, the main effects are separated into linear (L) and quadratic (Q), and the global binary interactions are described as linear−linear (L−L), linear−quadratic, quadratic−linear (L−Q or Q−L), or quadratic−quadratic (Q−Q). Higher-order interactions are usually negligible.[38] The sum of squares and medium squares are denoted by SS and MSS, respectively, for the diverse sources of variation. The ratio of the MSS of the variation source relative to that of the error is F_o. A comparison of the F_o value with the critical F-significance value test, in the form of $F_{(1\text{-alpha},\ \upsilon 1,\upsilon 2)}$, allowed the determination of whether a given source of variation is significant or not. Alpha is the probability level (95% in all cases), υ_1 denotes the degrees of freedom (DF) of the source of variation, and υ_2 indicates the DF of the error. The values of $F_{(1\text{-alpha},\ \upsilon 1,\upsilon 2)}$ also apply to the ANOVA results included in the Supporting Information for the corresponding sources of variation.

Table 1. ANOVA Results for Ethane Conversion (%)[a]

source of variation	SS	DF	MSS	F_o	F critical at 95%
W[b]	2057.6	2	1028.8	2052.4	3.55
W_L	2057.0	1	2056.9	4103.6	4.41
W_Q	0.68	1	0.67	1.35	4.41
T[c]	11 623.7	2	5811.8	11 594.5	3.55
T_L	11 623.7	1	11 623.7	23 189.0	4.41
T_Q	0.02	1	0.02	0.04	4.41
$T-W$ interactions	61.6	4	15.4	30.7	2.93
W_L-T_L	46.9	1	46.9	93.6	4.41
W_L-T_Q	14.4	1	14.4	28.7	4.41
W_Q-T_L	0.31	1	0.31	0.62	4.41
W_Q-T_Q	0.0011	1	0.001	0.002	4.41
error	9.0	18	0.501	1.00	
total	13 752.1	26	528.9	1055.2	

[a]SS, DF, and MSS denote sum of squares, degrees of freedom, and medium sum of squares, respectively. [b]W stands for space−time $(w_{cat}F_{ethane,o}^{-1})$. [c]$T$ represents temperature (°C).

Specific information obtained from the ANOVA for ethane conversion is shown in Table 1. There, observe that the Q effect of both space−time (W) and temperature (T) is not significant; even though the W_L-T_L interaction is significant at the 95% probability, its F_o value is relatively low, suggesting a marginal influence on the response.

In the case of the selectivities for ethylene and CO_x presented in the Supporting Information, the Q effect of space−time influences significantly the response's values, contrary to what occurs with W_Q. In the case of the STY of ethylene shown in the Supporting Information, both W_Q and T_Q effects appear to be statistically significant, although the former exhibits a slightly larger value of F_o, compared to the critical F value.

It is generally seen from the ANOVA results of the four studied responses that the W_L and T_L effects have the largest influence among the variation sources. The W_L-T_L interaction is significant; conversely, the W_Q-T_L and W_Q-T_Q interactions are not significant at the 95% level of probability. Also, it is observed that the F_o value of the W_L-T_Q interaction is relatively low, indicating little influence from this interaction on the considered responses.

3.3.3. Regression Analysis and Surface Responses. The next step in the analysis of the experimental design information is the proposal of a mathematical model, which is of great utility for prediction purposes. Such models, correlating the value of a given response with the factors involved, could be utilized for optimization purposes, namely, as a tool to estimate the values of the factors that maximize (or minimize) a specific response.[37]

In this work, a multiple nonlinear regression analysis of the catalytic responses, obtained from the experimental design data, was carried out to build models. Said analysis allows prediction of the value of the responses to combinations of temperature and space−time within the experimental design region. For the sake of brevity, particular examples are offered for ethane conversion, ethylene selectivity, and the STY of ethylene as responses. On the basis of a previous assessment of the main effects and the interactions of factors via an ANOVA, a second order polynomial, with the general form represented by eq 20, was found to be suitable and general enough to represent the relation between a dependent variable or response $(\hat{Y})$ and the independent variables (x_i).

$$\hat{Y} = a_o + \sum_{i=1}^{k} a_i x_i + \sum_{i=1}^{k} a_{ii} x_i^2 + \sum_i \sum_j a_{ij} x_i x_j \qquad (20)$$

The values of a_1, a_2, a_{11}, ..., are closely linked with linear effects (a_i), quadratic effects (a_{ii}), and interactions (a_{ij}) between factors. Hence, eq 20 may be simplified when there exists evidence that effects and/or interactions are not statistically significant for a given response. For instance, eq 20 takes the form of eq 21 for predicting the value of response $\hat{Y}$ as a function of temperature (T) and space−time (W) with a_0, a_1, a_2, a_{11}, and so forth as parameters to be estimated via regression from the experimental design data.

$$\hat{Y} = a_0 + a_1 T + a_2 W + a_{11} T^2 + a_{12} TW + a_{22} W^2 \qquad (21)$$

Table 2 displays the values of the estimates for parameters a_0, a_1, a_2, a_{11}, ..., including the corresponding 95% probability confidence intervals. Also, some statistical information is included for the models proposed for ethane conversion, ethylene selectivity, and CO_x selectivity along with the STY of ethylene, for which only the statistically significant parameters have been accounted. The models were adequate to predict the

dx.doi.org/10.1021/ie402447h | Ind. Eng. Chem. Res. XXXX, XXX, XXX−XXX

Table 2. Statistically Significant Main Parameters Values with 95% Confidence Intervals Related to Equation 21 Proposed to Fit Ethane Conversion, Ethylene Selectivity, CO*x* Selectivity, and STY of Ethylene

	response			
parameter	ethane conversion, %	ethylene selectivity, %	CO*x* selectivity, %	STY, $g_{ethylene}$ $(h\ kg_{cat})^{-1}$
a_0	$(-2.51 \pm 0.094) \times 10^{2}$	$(-3.08 \pm 0.33) \times 10^{-1}$	$(-4.06 \pm 0.31) \times 10^{2}$	$(-2.87 \pm 0.33) \times 10^{3}$
a_1	$(6.35 \pm 0.21) \times 10^{-1}$	$(1.90 \pm 0.15) \times 10^{0}$	$(-1.89 \pm 0.14) \times 10^{0}$	$(7.84 \pm 0.73) \times 10^{0}$
a_2	$(4.55 \pm 0.36) \times 10^{-1}$	$(9.91 \pm 0.91) \times 10^{-1}$	$(-9.90 \pm 0.81) \times 10^{-1}$	$(3.06 \pm 0.73) \times 10^{1}$
a_{11}		$(-2.22 \pm 0.17) \times 10^{-3}$	$(2.21 \pm 0.17) \times 10^{-3}$	
a_{22}				$(-9.01 \pm 1.47) \times 10^{-2}$
a_{12}		$(-2.54 \pm 0.21) \times 10^{-3}$	$(2.54 \pm 0.21) \times 10^{-3}$	$(5.20 \pm 0.35) \times 10^{-2}$
F_{reg}	2300	2726	2726	303
SS_{reg}	13 680	1146	1146	647 330
SS_{error}	71.3	2.3	2.3	11 738
R^2	0.9940	0.9976	0.9976	0.9790

cited responses on the basis of the determination coefficient (R^2) and the *F*-value, while other tests (e.g., residuals distribution) were, for practical reasons, not included.

For ethane conversion, parameters a_0, a_1, and a_2 were statistically significant, indicating and confirming that the pure interaction terms (a_{ij}) along with the quadratic effects (a_{ii}) do not impact the model predictions. In other words, a linear model with temperature and space−time suffices to describe ethane conversion. In the cases of ethylene selectivity, CO_x selectivity, and the STY of ethylene, models suitable for describing these responses are clearly nonlinear. For the selectivity of ethylene and CO_x, the information in Table 2 indicates that all parameters, except for a_{22}, were statistically significant, implying that the quadratic effect of space−time does not influence these responses. For the STY of ethylene, in contrast, the term a_{11} was not statistically significant; therefore, the quadratic effect of temperature was negligible. All these results are in a good agreement with the information provided by the ANOVA results, that is, the analytical assessment of the main effects and interactions as well as the graphical analysis of interactions.

The models discussed in the previous paragraphs were used to construct 3D plots, namely, surface responses, from which the variations of values such as ethane conversion, ethylene selectivity, and the STY of ethylene that result from the simultaneous changes of temperature and space−time are observed. Surface responses are also useful to identify regions of convenient operation. Figure 7 contains the 3D plots of ethane conversion and ethylene selectivity, while Figure 8 includes the corresponding plots for CO_x selectivity and the STY of ethylene. The topography of the surface varies among responses; specifically, the ethane conversion 3D plot corresponds to a hillside, while the plots associated not only with the STY of ethylene but also the selectivity for ethylene and CO_x seem to be saddle surface responses.

From a visual inspection of these graphs, the region of largest selectivity for ethylene (Figure 7b) requires operation at low temperature and space−time, whereas operating in the opposite direction clearly favors the formation of undesirable CO_x. Low temperature and space−time operation, however, leads to very low ethane conversions (Figure 7a). Besides, attractive values of the STY of ethylene (Figure 8b) are achieved when moving to high temperature and low space−time values.

3.4. Ethane and Oxygen Inlet Partial Pressure Effect. Kinetic orders were computed by using the set of experiments in which the ethane and oxygen inlet partial pressures were varied. Figure 9 shows the plots of the overall rate of ethane,

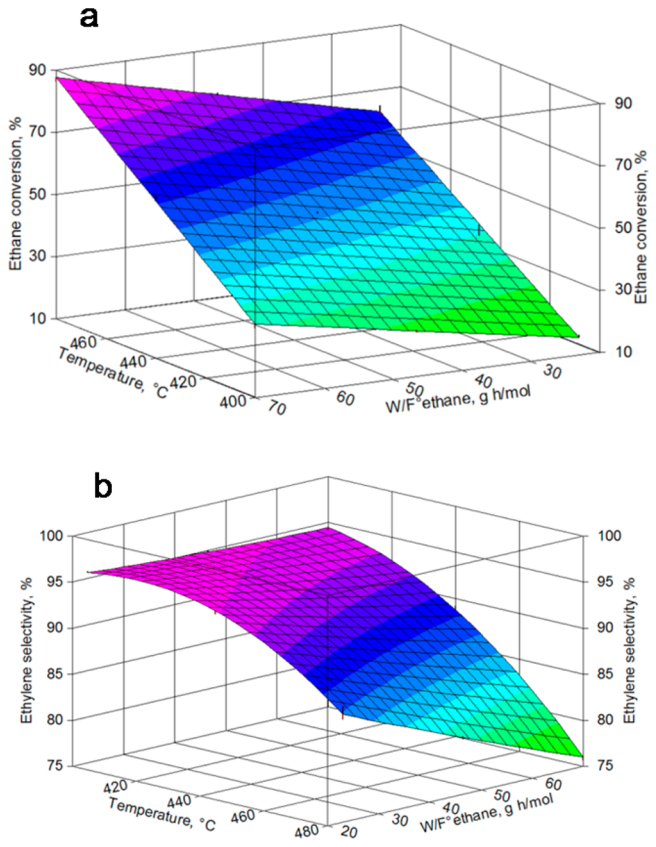

Figure 7. 3D response surfaces for (a) ethane conversion and (b) ethylene selectivity. Plots were constructed from the model fitted using the experimental design data. Temperature varied from 400 to 480 °C; space−time ranged between 23 and 70 g_{cat} h (mol of ethane)$^{-1}$; inlet molar ratio $C_2/O_2/N_2$ = 9/7/84.

ethylene, CO_2, and CO as a function of ethane and oxygen inlet partial pressures. Observe that the overall production rate of the various species varies linearly with the inlet partial pressure of both ethane and oxygen. In all plots, however, the slope of the straight line resulting from varying the inlet partial pressure of ethane is greater than that resulting from adjusting the inlet partial pressure of oxygen. Therefore, the overall production rate of the species mentioned above is more sensitive to changes in the inlet partial pressure of ethane than it is to changes in the inlet partial pressure of oxygen. Consequently, the kinetic orders associated with the inlet partial pressure of oxygen are expected to exhibit lower absolute values.

dx.doi.org/10.1021/ie402447h | *Ind. Eng. Chem. Res.* XXXX, XXX, XXX−XXX

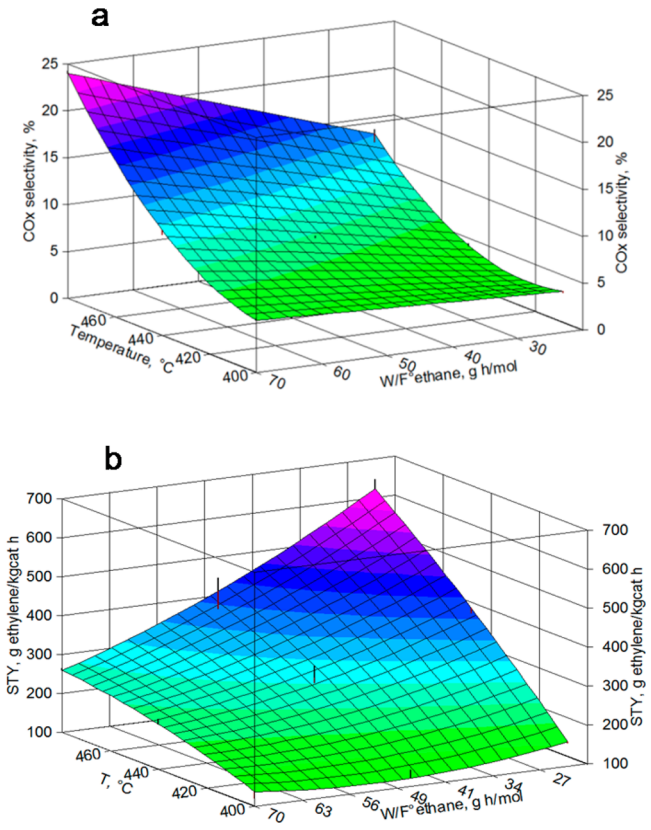

Figure 8. 3D response surfaces for (a) CO_x selectivity and (b) STY of ethylene. Plots were constructed from the model fitted using the experimental design data. Temperature varied from 400 to 480 °C; space−time ranged between 23 and 70 g_{cat} h (mol of ethane)$^{-1}$; inlet molar ratio $C_2/O_2/N_2$ = 9/7/84.

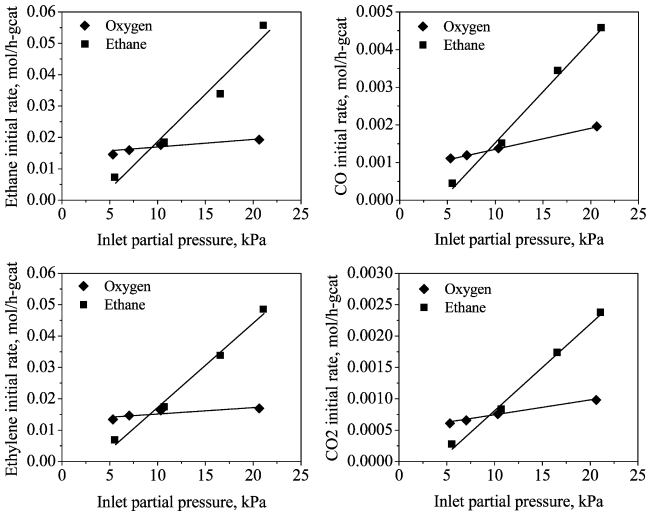

Figure 9. (counterclockwise from upper left) Overall rate of ethane, ethylene, CO_2, and CO as a function of the partial pressures of ethane and oxygen. $T_{reaction}$ = 440 °C; ethane (or oxygen) inlet partial pressure ranged from 5.1 to 22.3 kPa; space−time ranged between 10 and 140 g_{cat} h (mol of ethane)$^{-1}$.

The computed kinetic orders associated with the oxygen partial pressure are appreciably lower than 1.0, corresponding to 0.17, 0.36, and 0.43 for the overall rates of ethylene, CO_2, and CO, respectively. The kinetic orders related to ethane, in contrast, were systematically above 1.0, amounting to 1.46, 1.61, and 1.76 for the overall rates of ethylene, CO_2, and CO, respectively. These results indicate that, over the MoVTeNb mixed-oxide catalyst, the overall rates are substantially more dependent on the inlet partial pressure of hydrocarbon than on that of oxygen. In fact, the reaction producing ethylene is less sensitive to the oxygen partial pressure than is the combustion reaction involved in CO_x formation. These results are, particularly for the kinetic orders related to oxygen, in good agreement with previous reports.[26,27,29] For the corresponding overall rates, Kaddouri et al.[29] reported kinetic orders of 0.16, 0.17, and 0.25 for oxygen and 1.0, 1.14, and 1.35 for ethane, from lab-scale experiments over a β-$NiMoO_4$ catalyst. Also, Lemonidou et al.[27] reported oxygen partial pressure reaction orders of 0.21 and 0.83 for the reactions of ethylene and CO_2 formation, respectively, on a Ni−Nb based catalyst. For the same two reactions, Klose et al.[26] obtained values of 0.02 and 0.24 over a VO_x/γ-Al_2O_3 catalyst.

That the reaction (kinetic) orders associated with hydrocarbons are substantially larger than those associated with oxygen indicates that these reaction rates are much more sensitive to the partial pressure of hydrocarbons (ethane and ethylene). In other words, small changes in the partial pressure of hydrocarbons may have an appreciable impact on the reaction rate, contrary to what occurs in the case of oxygen. The low values of the reaction orders associated with the partial pressure of oxygen suggest that reaction occurs over the oxygen associated with the solid rather than the oxygen in the gas phase. Indeed, this result is in agreement with a Mars−Van Krevelen redox mechanism, in which the labile oxygen species on a catalyst are easily available, and the catalyst's reoxidation is faster. Therefore, the higher reaction order for ethane will have a beneficial effect on the STY of ethylene.

3.5. Apparent Kinetics: Model Parameters and Performance. Table 3 shows reparameterized pre-exponential factors, activation energies, and reaction orders, including their corresponding 95% probability confidence intervals, obtained by regression for the power law kinetic model. Notice that the parameters for the oxidation of ethylene to CO_2, according to the reaction network of Scheme 1, are not reported, as the corresponding activation energy could not be estimated with statistical significance. This indicates that CO_2 is most likely formed from ethane, and CO is produced from both ethane and ethylene. Reaction orders were estimated using the values of the kinetic orders reported in section 3.4 as initial estimations. The initial values of the reaction orders associated with the secondary reactions of CO_x formation from ethylene were obtained via the regressions of $\ln(R^{o}_{CO_x})$ vs $\ln(P^{o}_{O_2})$ as well as $\ln(R^{o}_{CO_x})$ vs $\ln(P_{ethylene})$ using experimental data, following a methodology similar to that described earlier.

Observe in Table 3 that the reaction responsible for the formation of ethylene exhibited the lowest activation energy (119 kJ mol^{-1}). The reoxidation of ethylene to CO, in contrast, demanded the largest amount of activation energy (242 kJ mol^{-1}). Over the catalyst investigated in this work, reactions involving the formation of CO_x species required more energy than the desired reaction leading to the formation of ethylene. Among the oxidation reactions considered in the kinetic model, ethane to CO demanded the lowest activation energy (143 kJ mol^{-1}). Additionally, the fact that oxidation reactions exhibit a larger activation energy than the partial oxidation (i.e., ethylene formation) indicates that an increased temperature favors oxidation reactions to produce CO_x.

dx.doi.org/10.1021/ie402447h | Ind. Eng. Chem. Res. XXXX, XXX, XXX−XXX

Table 3. Nonisothermal Parameters Results Containing Reparameterized Pre-exponential Factors and Activation Energies with Corresponding 95% Probability Confidences[a]

reaction	A_{rep}, mol $(g_{cat}\ h\ kPa^{\alpha+\beta})^{-1}$	E, kJ mol^{-1}	α_i[b]	β_i[c]
$C_2H_6 + 0.5O_2 \rightarrow C_2H_4 + H_2O$	$5.34 \times 10^{-4} \pm 2.97 \times 10^{-5}$	119 ± 12.6	1.50	0.13
$C_2H_6 + 3.5O_2 \rightarrow 2CO_2 + 3H_2O$	$7.44 \times 10^{-6} \pm 1.24 \times 10^{-6}$	217 ± 33.1	1.78	0.36
$C_2H_6 + 2.5O_2 \rightarrow 2CO + 3H_2O$	$1.37 \times 10^{-5} \pm 1.53 \times 10^{-6}$	143 ± 53.2	1.80	0.24
$C_2H_4 + 2O_2 \rightarrow 2CO_2 + 2H_2O$		n.r.[d]		
$C_2H_4 + 2O_2 \rightarrow 2CO + 2H_2O$	$3.38 \times 10^{-5} \pm 3.95 \times 10^{-6}$	242 ± 37.8	1.33	0.30

[a] F_{reg} = 542.9, F_{tab} = 2.79, t_{tab} = 1.97 at 1-alpha = 0.95 and 244 degrees of freedom. [b] α_i = reaction order associated with the partial pressure of ethane for reaction i. [c] β_i = reaction order associated with the partial pressure of oxygen for reaction i. [d] n.r. = not reported as parameters were not statistically significant.

On the basis of the information included in Table 3, the values of the reparameterized pre-exponential factor, $A_{rep,i}$, which actually correspond to the rate coefficient of reaction i computed at T_m, evolve as follows: ethylene > CO from ethylene > CO from ethane > CO_2 from ethane. At T_m, $A_{rep,i}$ for ethylene production is two orders of magnitude larger than that for the formation of CO_2 from ethane. This trend is qualitatively in agreement with the results discussed in a previous section, since the highest pre-exponential value for ethylene formation is associated with the high selectivity for ethylene shown by the catalyst. This selectivity is related to the high amount of active surface sites participating in the ODH of ethane to selectively produce ethylene. By contrast, the very low selectivity for CO_x indicates that the catalyst exhibits a minimum amount of active sites for those reactions.

The main values of the pre-exponential factor (A) in mol $(g_{cat}\ h\ kPa^{\alpha+\beta})^{-1}$ were calculated from reparameterized pre-exponential factors included in Table 3 with a T_m equal to 440 °C. Thus, for the four reactions with statistically significant parameter values, A amounted to 2.8×10^5, 6.2×10^{10}, 3.9×10^5, and 1.7×10^{13} mol $(g_{cat}\ h\ kPa^{\alpha+\beta})^{-1}$, respectively. Notice that the pre-exponential factor of the first reaction is 8 orders of magnitude smaller than the one of the fourth reaction. In general, the values of the pre-exponential factors evolve in an opposite direction compared with activation energies, as the reaction with the highest value of activation energy (242 kJ mol^{-1} for CO formation from ethylene) exhibited the largest pre-exponential factor. It is clear that the differences in the magnitude orders of pre-exponential factors compensate for the detected deviations in the values of the activation energies.

The corresponding main values of the reaction orders for the four reactions with statistically significant parameters in accordance with Table 3 were, from top to bottom, 1.50, 1.78, 1.80, and 1.33 for the partial pressures of hydrocarbons and 0.13, 0.36, 0.24, and 0.30 for the partial pressures of oxygen. Evidently, all the reaction rates composing the kinetic model exhibit very low dependence on the oxygen partial pressure, contrary to what occurs with the partial pressures of hydrocarbons. As mentioned before, the effect observed for the oxygen concentration is in agreement with information outlined in other publications.[26,27]

The F-test was used to verify the model adequacy and the global significance of the regression. Table 3 reports a value of F_{reg} equal to 460; F_{tab} amounted to 2.79 for 244 degrees of freedom and 95% probability.

Finally, parity diagrams were constructed in order to compare the experimental data to the corresponding data predicted by the kinetic model. Figure 10, panels a and b compare the experimental and the predicted ethane and oxygen conversions, while Figure 10, panels c and d contrast the experimental and the predicted ethylene and CO_x molar yields. Note that the model predictions for both reactant conversion and product yield describe very well the kinetic phenomena occurring on the MoVTeNb mixed-oxide catalyst.

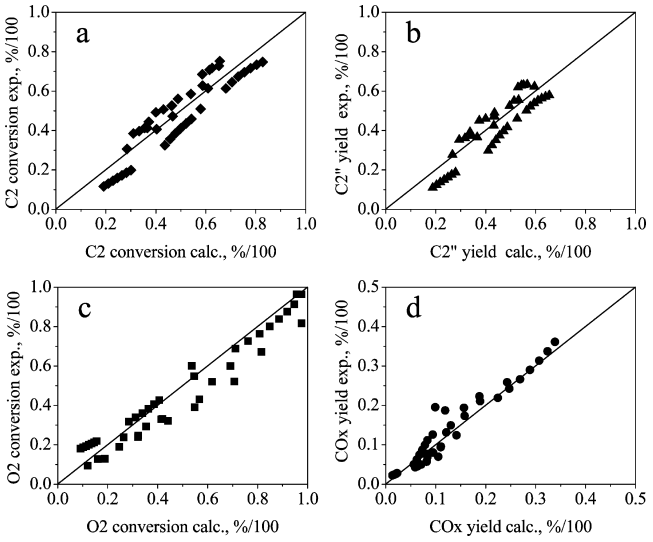

Figure 10. Parity plots showing calculated versus experimental percent conversions of (a) ethane and (c) oxygen and product yields of (b) ethylene and (d) CO_x. Conversions and yields were computed with a power law kinetic model.

4. CONCLUSIONS

In this work, the effects of temperature (T) and space−time (W) on the catalytic performance of a MoVTeNb mixed-oxide catalyst for the ODH of ethane were investigated by means of a set of experiments included in a 3^k experimental design. The main linear effects of T and W on ethane conversion were observed without detection of any interaction between these two factors. In contrast, the main effects of T and W are not linear on the selectivity for ethylene or CO_x, while an interaction between T and W is observed. Ethane conversion is clearly enhanced at high values of both T and W although, under these conditions, CO_x production rises, to the detriment of ethylene formation. Operation at high temperature and low space−time is convenient for obtaining high values of the STY of ethylene, a key parameter from the industrial point of view. Actually, under the conditions studied here, namely, the process variables and the catalyst formulation, the highest value of the STY of ethylene, amounting to ∼640 $g_{ethylene}$ $(kg_{cat}\ h)^{-1}$, is detected at the highest temperature (480 °C) and the lowest space−time (23 g_{cat} h mol^{-1}).

dx.doi.org/10.1021/ie402447h | Ind. Eng. Chem. Res. XXXX, XXX, XXX−XXX

Experiments varying the inlet partial pressures of ethane and oxygen indicated a very low dependency of the overall rate of formation of the various product species, in particular that leading to ethylene, on the inlet partial pressure of oxygen, with experimental kinetic orders within the range of 0.17−0.43.

Kinetic modeling indicates that CO_2 is mainly formed from ethane, while CO is produced from both ethane and ethylene and exhibits low values of reaction orders associated with the partial pressure of oxygen. Kinetic information also indicates that the reaction to form ethylene has the lowest demand for energy (119 kJ mol^{-1}), while the oxidation of ethylene to CO requires the highest amount of energy (242 kJ mol^{-1}). The pre-exponential factors of the most energy-demanding reaction are, in general, several orders of magnitude higher than those of the other reactions, thus partially compensating the existing differences in values of activation energies.

■ ASSOCIATED CONTENT

Supporting Information

The main physicochemical properties of the material and ANOVA results for ethylene selectivity, CO_x selectivity, and the STY of ethylene. This material is available free of charge via the Internet at http://pubs.acs.org.

■ AUTHOR INFORMATION

Corresponding Authors

*E-mail: jsanchez@imp.mx (J.S.V.) Tel.: +52 55 9175 8444.
*E-mail: rquintana@imp.mx (R.Q.S.) Tel.: +52 55 9175 8530.

Notes

The authors declare no competing financial interest.

■ ACKNOWLEDGMENTS

This work was financially supported by the Instituto Mexicano del Petroleo. Technical support from Eng. G. Alonso-Ramirez is gratefully acknowledged.

■ NOMENCLATURE

Symbols

A_i = chromatographic area of species i
A_i = pre-exponential factor for reaction i, mol $(g_{cat}\ h\ kPa^{\alpha+\beta})^{-1}$
$A_{rep,i}$ = reparameterized pre-exponential factor for reaction i, mol $(g_{cat}\ h\ kPa^{\alpha+\beta})^{-1}$
C_2 = ethane
CO_x = CO_2 + CO
Cf_i = GC calibration factor for species i
$C_{atoms,i}$ = carbon atoms number composing compound i
STY = space time yield of ethylene, $g_{ethylene}$ $(kg_{cat}\ h)^{-1}$
$G^o_{C,ethane}$ = reactor inlet mass flow of the carbon associated with ethane, g h^{-1}
$G_{C,ethane}$ = reactor outlet mass flow of the carbon associated with ethane, g h^{-1}
E_i = apparent activation energy of reaction i, kJ mol^{-1}
F^o_i = reactor inlet molar flow rate of species i, mol h^{-1}
F_i = reactor outlet molar flow rate of species i, mol h^{-1}
j = species, experiment or reaction
i = species, experiment or reaction
L = linear effect
L−L = linear to linear interaction between pair of factors
L−Q = linear to quadratic interaction between pair of factors
k = number of factors in the experimental design
k_i = rate coefficient of reaction i, mol $(g_{cat}\ h\ kPa^{\alpha+\beta})^{-1}$
M_i = molecular mass of species i
m_j = kinetic order related to the partial pressure of ethane
n_{obs} = number of independent experiments
n_p = number of kinetic parameters included in the objective function
n_{resp} = number of responses per experiment
N_2 = nitrogen
n_j = apparent kinetic order related to the partial pressure of oxygen
n_r = number of reactions
O_2 = oxygen
P^o_i = inlet partial pressure of species i, kPa
P_i = partial pressure of species i, kPa
Q = quadratic effect
Q−Q = quadratic to quadratic interaction between factors
R_i = net rate of production (or overall rate) of species i, mol $(g_{cat}\ h)^{-1}$
r_i = rate of reaction i, mol $(g_{cat}\ h)^{-1}$
RSS = residual sum of squares
$S_{C,i}(t)$ = selectivity for product i on carbon basis, %
T = temperature, °C
t = time, min or h
T_m = average temperature, K
w_{cat} = mass of catalyst, g
$w_{cat}F_{ethane,o}^{-1}$ = space−time, g_{cat} h (mol of ethane)$^{-1}$
w_j = weight factor in the objective function
W = space−time (notation reserved for the experimental design), g_{cat} h (mol of ethane)$^{-1}$
$X_{c,ethane}$ = ethane conversion on carbon basis, %
$\hat{Y}_{i,j}$ = predicted yields, mol of species i (mol of ethane)$^{-1}$
Y_{ij} = experimental molar yields designated, mol of species i (mol of ethane)$^{-1}$
x_i = independent variable included in the regression model

Greek Symbols

α_i = reaction order associated with the partial pressure of ethane for reaction i
β_i = reaction order associated with the partial pressure of oxygen for reaction i
β = vector of parameters accounted for in the objective function

■ REFERENCES

(1) Lippe, D. Ethylene Markets Return to Normal. *Oil Gas J.* **2011**, *109−10*, 94.
(2) Bhasin, M. M. Is True Ethane Oxydehydrogenation Feasible? *Top. Catal.* **2003**, *23* (1−4), 145.
(3) Sanfilippo, D.; Miracca, I. Dehydrogenation of Paraffins: Synergies between Catalyst Design and Reactor Engineering. *Catal. Today* **2006**, *111* (1−2), 133.
(4) Grabowski, R. Kinetics of Oxidative Dehydrogenation of C−C_3 Alkanes on Oxide Catalysts. *Catal. Rev.* **2006**, *48−2*, 199.
(5) Cavani, F.; Ballarini, N.; Cercola, A. Oxidative Dehydrogenation of Ethane and Propane: How Far from Commercial Implementation? *Catal. Today* **2007**, *127*, 113.
(6) Bhasin, M. M.; McCain, J. H.; Vora, B. V.; Imai, T.; Pujado, P. R. Dehydrogenation and Oxydehydrogenation of Paraffins to Olefins. *Appl. Catal., A* **2001**, *221*, 397.
(7) Lange, J. P.; Schoonebeek, R. J.; Mercera, P. D. L.; van Breukelen, F. W. Oxycracking of Hydrocarbons: Chemistry, Technology and Economic Potential. *Appl. Catal., A* **2005**, *283*, 243.
(8) Ruth, K.; Kieffer, R.; Burch, R. Mo−V−Nb Oxide Catalyst for the Partial Oxidation of Ethane. *J. Catal.* **1998**, *175*, 16.
(9) Gärtner, C. A.; van Veen, A. C.; Lercher, J. A. Oxidative Dehydrogenation of Ethane: Common Principles and Mechanistic Aspects. *ChemCatChem* **2013**, DOI: 10.1002/cctc.201200966.

(10) Hatano, M.; Kayo, A.; US 5,049,692, 1991, assigned to Mitsubishi Kasei Co.
(11) Lopez Nieto, J. M.; Botella, P.; Vázquez, M. I.; Dejoz, A. The Selective Oxidative Dehydrogenation of Ethane over Hydrothermally Synthesised MoVTeNb Catalysts. *Chem. Commun.* **2002**, 1906.
(12) Lopez Nieto, J. M.; Botella, P.; Vázquez, M. I.; Dejoz, A. WO 03/064035 A1, 2003, assigned to CSIC-UPV.
(13) Lopez Nieto, J. M.; Botella, P.; Vázquez, M. I.; Dejoz, A. US 7,319,179 B2, 2008, assigned to CSIC-UPV.
(14) Solsona, B.; Vázquez, M. I.; Ivars, F.; Dejoz, A.; Concepción, P.; Lopez Nieto, J. M. Selective Oxidation of Propane and Ethane on Diluted Mo−V−Nb−Te Mixed-Oxide Catalysts. *J. Catal.* **2007**, *252*, 271.
(15) Nguyen, T. T.; Burel, L.; Nguyen, D. L.; Pham-Huu, C.; Millet, J. M. M. Catalytic Performance of MoVTeNbO Catalyst Supported on SiC Foam in Oxidative Dehydrogenation of Ethane and Ammoxidation of Propane. *Appl. Catal., A* **2012**, *433*, 41.
(16) Xie, Q.; Chen, L.; Weng, W.; Wan, H. Preparation of MoVTe(Sb)Nb Mixed-Oxide Catalysts Using a Slurry Method for Selective Dehydrogenation of Ethane. *J. Mol. Catal. A: Chem.* **2005**, *240*, 191.
(17) Nguyen, T. T.; Aouine, M.; Millet, J. M. M. Optimizing the Efficiency of MoVTeNbO Catalysts for Ethane Oxidative Dehydrogenation to Ethylene. *Catal. Commun.* **2012**, *21*, 22.
(18) Deniau, B.; Millet, J .M .M .; Loridanta, S.; Christin, N.; Dubois, J. L. Effect of Several Cationic Substitutions in the *M1* Active Phase of the MoVTeNbO Catalysts Used for the Oxidation of Propane to Acrylic Acid. *J. Catal.* **2008**, *260*, 30.
(19) DeSanto, P.; Buttrey, D. J.; Grasselli, R. K.; Lugmair, C. G.; Volpe, A. F.; Toby, B. H. Structural Characterization of the Orthorhombic Phase M1 in MoVNbTeO Propane Ammoxidation Catalyst. *Top. Catal.* **2003**, *23*, 23.
(20) Aouine, M.; Dubois, J. L.; Millet, J. M. M. Crystal Chemistry and Phase Composition of the MoVTeNbO Catalysts for the Ammoxidation of Propane. *Chem. Commun.* **2001**, 1180.
(21) Botella, P.; García-González, E.; Lopez Nieto, J. M.; González-Calbet, J. M. MoVTeNbO Multifunctional Catalysts: Correlation between Constituent Crystalline Phases and Catalytic Performance. *Solid State Sci.* **2005**, *7*, 507.
(22) Millet, J. M. M.; Baca, M.; Pigamo, A.; Vitry, D.; Ueda, W.; Dubois, J. L. Study of the Valence State and Coordination of Antimony in MoVSbO Catalysts Determined by XANES and EXAFS. *Appl. Catal., A* **2003**, *244*, 359.
(23) Deniau, B.; Bergeret, G.; Jouguet, B.; Dubois, J. L.; Millet, J. M. M. Preparation of Single M1 Phase MoVTe(Sb)NbO Catalyst: Study of the Effect of M2 Phase Dissolution on the Structure and Catalytic Properties. *Top. Catal.* **2008**, *50*, 33.
(24) Klose, F.; Wolf, T.; Thomas, S.; Seidel-Morgenstern, A. Operation Modes of Packed-Bed Membrane Reactions in the Catalytic Oxidation of Hydrocarbons. *Appl. Catal., A* **2004**, *257*, 193.
(25) Skoufa, S.; Heracleous, E.; Lemonidou, A. A. Investigation of Engineering Aspects in Ethane ODH over Highly Selective $Ni_{0.85}Nb_{0.16}O_x$ Catalyst. *Chem. Eng. Sci.* **2012**, *84*, 48.
(26) Klose, F.; Joshi, M.; Hamel, C.; Seidel-Morgenstern, A. Selective Oxidation of Ethane over a VO_x/γ-Al_2O_3 Catalyst—Investigation of the Reaction Network. *Appl. Catal., A* **2004**, *26*, 101.
(27) Lemonidou, A. A.; Heracleous, E. Ni−Nb−O Mixed Oxides as Highly Active and Selective Catalyst for Ethane Production via Ethane Oxidative Dehydrogenation. Part II: Mechanistic Aspects and Kinetic Modeling. *J. Catal.* **2006**, *237*, 175.
(28) Gaab, S.; Find, J.; Müller, T. E.; Lercher, J. A. Kinetics and Mechanism of the Oxidative Dehydrogenation of Ethane over Li/Dy/Mg/O/(Cl) Mixed-Oxide Catalysts. *Top. Catal.* **2007**, *46* (1−2), 101.
(29) Kaddouri, A.; Anouchinsky, R.; Mazzocchia, C.; Madeira, L. M.; Portela, M. F. Oxidative Dehydrogenation of Ethane on the α and β Phases of $NiMoO_4$. *Catal. Today* **1998**, *40* (2−3), 201.
(30) Malleswara-Rao, T. V.; Deo, G. Steady State Kinetic Parameters of Bulk V_2O_5 for Ethane and Propane Oxidation Reactions. *Catal. Commun.* **2007**, *8*, 957.
(31) Iglesia, E.; Argyle, M. D.; Chen, K.; Bell, A. T. Ethane Oxidative Dehydrogenation Pathways on Vanadium Oxide Catalysts. *J. Phys. Chem. B* **2002**, *106*, 5421.
(32) Grabowski, R.; Sloczynski, J. Kinetics of Oxidative Dehydrogenation of Propane and Ethane on VOx/SiO_2 Pure and with Potassium Additive. *Chem. Eng. Process.* **2005**, *44*, 1082.
(33) Mears, D. E. Test for Transport Limitations in Experimental Catalytic Reactors. *Ind. Eng. Chem. Process. Des. Dev.* **1997**, *10*, 541.
(34) Pérez-Ramírez, J.; Berger, R. J.; Mul, G.; Kapteijin, F.; Moulijin, J. A. The Six Flow Reactor Technology: A Review of Fast Catalyst Screening and Kinetic Studies. *Catal. Today* **2000**, *60*, 93.
(35) Petzold, L. R.; Hindmarsh, A. C. *ODEPACK Solver for Ordinary Differential Equations*; Lawrence Livermore National Laboratory: Livermore, CA, U.S.A., 1997.
(36) Boggs, P. T.; Byrd, R. H.; Rogers, J. E.; Schnabel, R. B. *ODRPACK 2.01 Software for Weighted Orthogonal Distance Regression*; National Institute of Standards and Technology: Gaithersburg, MD, U.S.A., 1992.
(37) Kremenic, G.; López-Nieto, J. M.; Tascón, J. M. D.; Tejuca, L. G.; Weller, S. W. Selective Oxidation of Propene on a MoPrBi Catalyst. *Ind. Eng. Chem. Res.* **1987**, *26*, 1419.
(38) Botella, P.; Dejoz, A.; Abello, M. C.; Vázquez, M. I.; Arrúa, L.; López Nieto, J. M. Selective Oxidation of Ethane: Developing an Orthorhombic Phase in Mo−V−X (X = Nb, Sb, Te) Mixed Oxides. *Catal. Today* **2009**, *142*, 272.
(39) Heynderickx, M. P.; Thybaut, J. W.; Poelman, H.; Poelman, D.; Marin, G. B. Kinetic Modeling of the Total Oxidation of Propane over $CuO-CeO_2/\gamma$-Al_2O_3. *Appl. Catal., B* **2010**, *95*, 26.
(40) Box, G. E. P.; Hunter, W. G.; Hunter, J. S. *Statistics for Experimenters: An Introduction to Design, Data Analysis and Model Building*; Wiley: Hoboken, NJ, U.S.A., 1978.
(41) Montgomery, D. C. *Design and Analysis of Experiments*; Wiley: Hoboken, NJ, U.S.A., 2000.
(42) Abdullah, S. B.; Juhari, J. Development and Optimization of $La_2O_3-ZnO-SnO_2$ Thick Film Catalytic Pellet for Detection of Carbon Monoxide. *J. Appl. Sci. Res.* **2008**, *4* (4), 415.
(43) Ekren, B. Y.; Ornek, A. M. A Simulation Based Experimental Design to Analyze Factors Affecting Production Flow Time. *Simul. Model. Pract. Theory* **2008**, *16*, 278.

dx.doi.org/10.1021/ie402447h | *Ind. Eng. Chem. Res.* XXXX, XXX, XXX−XXX